CRYSTAL GROWTH & DESIGN

Article

Cite This: *Cryst. Growth Des.* 2018, 18, 2555−2562

pubs.acs.org/crystal

Polycatenated 2D Hydrogen-Bonded Binary Supramolecular Organic Frameworks (SOFs) with Enhanced Gas Adsorption and Selectivity

Jian Lü,[†,‡,§] Cristina Perez-Krap,[§] Fabien Trousselet,[∥] Yong Yan,[⊥] Nada H. Alsmail,[§,#] Bahar Karadeniz,[†,§] Nicholas M. Jacques,[⊥] William Lewis,[§] Alexander J. Blake,[§] François-Xavier Coudert,[∥] Rong Cao,*[,‡] and Martin Schröder*[,⊥]

[†]Fujian Provincial Key Laboratory of Soil Environmental Health and Regulation, College of Resources and Environment, Fujian Agriculture and Forestry University, Fuzhou 350002, P. R. China

[‡]State Key Laboratory of Structural Chemistry, Fujian Institute of Research on the Structure of Matter, Chinese Academy of Sciences, Fuzhou 350002, P. R. China

[§]School of Chemistry, University of Nottingham, University Park, Nottingham NG7 2RD, U.K.

[∥]Chimie ParisTech, PSL Research University, CNRS, Institut de Recherche de Chimie Paris, 75005 Paris, France

[⊥]School of Chemistry, University of Manchester, Oxford Road, Manchester M13 9PL, U.K.

[#]Department of General Studies, Jubail University College, P.O. Box 10074, Jubail Industrial City 31961, SKA

Supporting Information

ABSTRACT: Controlled assembly of two-dimensional (2D) supramolecular organic frameworks (SOFs) has been demonstrated through a binary strategy in which 1,4-bis-(4-(3,5-dicyano-2,6-dipyridyl)pyridyl)naphthalene (**2**), generated *in situ* by oxidative dehydrogenation of 1,4-bis-(4-(3,5-dicyano-2,6-dipyridyl)dihydropyridyl)-naphthalene (**1**), is coupled in a 1:1 ratio with terphenyl-3,3′,4,4′-tetracarboxylic acid (**3**; to form **SOF-8**), 5,5′-(anthracene-9,10-diyl)diisophthalic acid (**4**; to form **SOF-9**), or 5,5′-bis-(azanediyl)-oxalyl-diisophthalic acid (**5**; to form **SOF-10**). Complementary O−H···N hydrogen bonds assemble 2D 6^3-**hcb** (honeycomb) subunits that pack as layers in **SOF-8** to give a three-dimensional (3D) supramolecular network with parallel channels hosting guest DMF (DMF = *N*,*N*′-dimethylformamide) molecules. **SOF-9** and **SOF-10** feature supramolecular networks of 2D → 3D inclined polycatenation of similar **hcb** layers as those in **SOF-8**. Although **SOF-8** suffers framework collapse upon guest removal, the polycatenated frameworks of **SOF-9** and **SOF-10** exhibit excellent chemical and thermal stability, solvent/moisture durability, and permanent porosity. Moreover, their corresponding desolvated (activated) samples **SOF-9a** and **SOF-10a** display enhanced adsorption and selectivity for CO_2 over N_2 and CH_4. The structures of these activated compounds are well described by quantum chemistry calculations, which have allowed us to determine their mechanical properties, as well as identify their soft deformation modes and a large number of low-energy vibration modes. These results not only demonstrate an effective synthetic platform for porous organic molecular materials stabilized solely by primary hydrogen bonds but also suggest a viable means to build robust SOF materials with enhanced gas uptake capacity and selectivity.

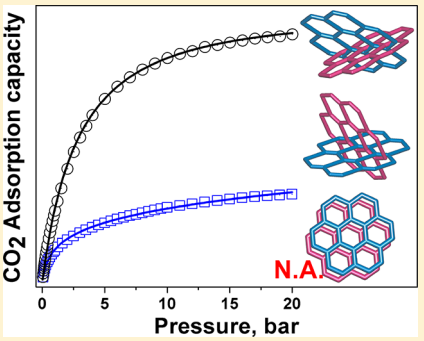

INTRODUCTION

Porous organic molecular solids have been proposed as a new platform of chemical materials. They tend to show low framework density resulting from being composed of light elements (typically limited to H, C, N, O, and B), and their synthesis can be achieved via controlled assembly using concepts from crystal engineering.[1−5] Various applications of porous organic molecular solids, including in catalysis, medicine, molecular sensing, storage, and separation,[6−10] depend on achieving designed architectures with predictable pore structures and the necessary functionality. However, the construction of porous organic molecular solids presents challenges in the delivery of required properties, including stable and permanent porosity, tailored pore structure, and functionality.

Supramolecular organic frameworks (SOFs),[11−18] which are structurally mimetic of the well-known metal organic frameworks (MOFs),[19−23] define porous crystalline molecular solids built from organic constituents assembled through supramolecular interactions. SOFs have shown promising applications in gas storage and separation.[24,25] The prevailing strategy for the construction of SOFs involves crystallization of a single organic constituent from an appropriate solvent system by exploiting supramolecular interactions such as hydrogen bonds,

Received: January 28, 2018
Published: February 16, 2018

DOI: 10.1021/acs.cgd.8b00153
Cryst. Growth Des. 2018, 18, 2555−2562

Scheme 1. Views of the Organic Components 1−5 and a Representative 6^3-hcb Net Observed in SOF 8−10

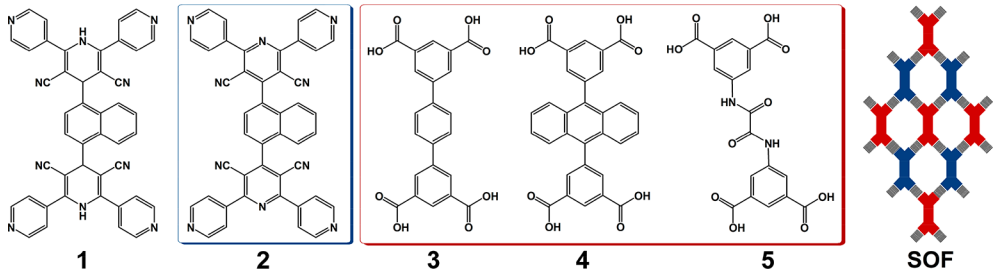

halogen bonds, and/or $\pi\cdots\pi$ interactions.[26−30] Given the "soft" and "flexible" nature of supramolecular interactions, as well as the numerous donating/accepting groups present, prediction of structures and controlled assembly of hydrogen-bonded SOFs in such single-component systems can be challenging.[30,31] We have now developed a binary design strategy,[25] which requires two types of organic constituents possessing separate complementary hydrogen bond donating and acceptor groups. The organic constituents should be chemically and geometrically adaptable to give intermolecular interactions that are optimized and balanced for assembly of binary SOF materials.[32]

The importance of dimensionality and well-defined in-plane crystallinity of two-dimensional (2D) materials is now well established,[28,29] and structural diversity of 2D molecular networks comes not only from the molecular assembly but also from the different packing arrangements possible for these nets.[29,33] In contrast to 3D SOFs,[12−18] 2D SOFs assembled solely through hydrogen bonds rarely exhibit both structural robustness and significant adsorption capacity in the solid state. With this in mind, we sought to construct thermally and chemically stable 2D SOF materials for selective adsorption of carbon dioxide (CO_2) using a new binary strategy. 1,4-Bis-(4-(3,5-dicyano-2,6-dipyridyl)dihydropyridyl)naphthalene (**1**) has been designed as a precursor for the generation of 1,4-bis-(4-(3,5-dicyano-2,6-dipyridyl) pyridyl)naphthalene (**2**) via *in situ* oxidative dehydrogenation.[25,34] We report that the combination of **2** with the tetracarboxylic acids terphenyl-3,3′,4,4′-tetracarboxylic acid, **3**, 5,5′-(anthracene-9,10-diyl)diisophthalic acid, **4**, or 5,5′-bis-(azanediyl)-oxalyl-diisophthalic acid, **5**, leads to the assembly of 2D binary SOF materials (Scheme 1). The *exo*-pyridyl (acceptors) and carboxyl (donors) groups on two separate organic constituents provide complementary and directional hydrogen bonding interactions for the assembly of porous structures with decorating phenyl, anthryl, or oxamide groups. Quantum chemistry calculations are used to determine the energetic and mechanical stability of the various frameworks synthesized here, as well as to analyze their elastic moduli and vibrational properties.

EXPERIMENTAL SECTION

Chemicals and General Methods. Commercially available reagents and organic solvents were used as received without further purification. 3-Amino-3-(4-pyridinyl)-propionitrile, naphthalene-1,4-dicarbaldehyde, terphenyl-3,3′,4,4′-tetracarboxylic acid, 5,5′-bis-(azanediyl)-oxalyl-diisophthalic acid, and 5,5′-(anthracene-9,10-diyl)-diisophthalic acid were prepared according to the reaction procedures previously described in the literature; naphthalene-1,4-dicarbaldehyde was synthesized using an adapted method reported previously.[35,36]

Elemental analyses (C, H, and N) were performed on a CE-440 elemental analyzer. Infrared (IR) spectra were recorded with a PerkinElmer Spectrum One instrument as KBr pellets in the range 400−4000 cm^{-1}, or on a Nicolet is5 FT-IR spectrophotometer in the range 550−4000 cm^{-1} using attenuated total reflectance (ATR) mode. ^1H NMR spectra were recorded on a Bruker DPX-400 spectrometer. Thermal gravimetric analyses (TGA) were performed under a flow of N_2 (20 mL min^{-1}) with a heating rate of 10 °C min^{-1} using a TA SDT-600 thermogravimetric analyzer. Powder X-ray diffraction (PXRD) measurements were carried out at room temperature on a PANalytical X'Pert PRO diffractometer using Cu Kα radiation (λ = 1.5418 Å) and generator settings of 40 kV, 40 mA, at a scan speed of 0.02°/s and a step size of 0.005° in 2θ. CO_2, N_2, and CH_4 isotherms were recorded using an IGA gravimetric adsorption apparatus (Hiden) at the University of Nottingham in a clean ultra-high-vacuum system with a diaphragm and turbo pumping system. Before measurement, about 60 mg of solvent-exchanged sample was loaded into the sample basket within the adsorption instrument and then degassed under dynamic vacuum at 100 °C for 24 h to obtain fully desolvated samples.

Synthesis of 1,4-Bis-(4-(3,5-dicyano-2,6-dipyridyl)-dihydropyridyl)naphthalene (1). 3-Amino-3-(4-pyridinyl)-propionitrile (580 mg, 4.0 mmol) and naphthalene-1,4-dicarbaldehyde (184 mg, 1.0 mmol) were added to acetic acid (10 mL) under N_2 and the reaction mixture refluxed at 120 °C for 48 h. The light yellow precipitate of **1** was collected by filtration and washed with hot acetic acid, EtOH, and distilled water and dried in air. Yields: *ca.* 51%. ^1H NMR (DMSO-d^6): 10.51 (s, 2H, dihydropyridyl-NH); 8.77 (d, J = 5.9 Hz, 8H, Py-H); 8.68 (dd, J = 9.9, 5.4 Hz, 2H, naphthyl-H); 7.99 (d, J = 5.8 Hz, 2H, naphthyl-H); 7.76 (dd, J = 6.5, 3.2 Hz, 2H, naphthyl-H); 7.71 (dd, J = 12.7, 9.8 Hz, 8H, Py-H); 5.93 (s, 2H, dihydropyridyl-CH) ppm. IR (KBr, υ_{max}, cm^{-1}): 2206 (s), 1643 (m), 1578 (w), 1550 (m), 1475 (s), 1406 (m), 1390 (m), 1339 (w), 1290 (s), 1221 (w), 1189 (w), 1153 (m), 1068 (w), 996 (m), 851 (s). Elemental analysis for $C_{44}H_{26}N_{10}$ (found/calcd): C, 74.02/76.07; H, 3.69/3.77; N, 19.78/20.16%.

Synthesis of SOF 8−10. 1,4-Bis-(4-(3,5-dicyano-2,6-dipyridyl)-dihydropyridyl)naphthalene (**1**) (35 mg, 0.05 mmol) and terphenyl-3,3′,4,4′-tetracarboxylic acid (**3**) (21 mg, 0.05 mmol) were added into 3 mL of DMF. The reaction mixture was transferred into a 15 mL pressure tube and heated in oil bath at 90 °C and autogenous pressure for 3 days. Orange crystals were collected by filtration and washed with cold DMF to give the pure phase of **SOF-8** (yield: *ca.* 32%). **SOF-9** and **SOF-10** were prepared in similar reactions using 5,5′-bis-anthrathene-diisophthalic acid (**4**) (26 mg, 0.05 mmol) and 5,5′-bis-(azanediyl)-oxalyl-diisophthalic acid (**5**) (21 mg, 0.05 mmol) instead of **3** (in yields of *ca.* 29% and *ca.* 36%, respectively). The composition and amount of included solvent molecules in **SOF 8−10** were determined by elemental analyses, TGA results, and the electron densities calculated from the PLATON/SQUEEZE routine,[37] which give optimized formulae of $[(C_{22}H_{14}O_8)\cdot(C_{44}H_{22}N_{10})]\cdot 3DMF$ (**SOF-8**), $[(C_{30}H_{18}O_8)\cdot(C_{44}H_{22}N_{10})]\cdot 7DMF$ (**SOF-9**), and $[(C_{18}H_{12}N_2O_{10})\cdot(C_{44}H_{22}N_{10})]\cdot 6DMF$ (**SOF-10**). Elemental analysis for **SOF-8** ($C_{75}H_{57}N_{13}O_{11}$; found/calcd): C, 68.77/68.44; H, 4.09/4.36; N, 13.04/13.83%; for **SOF-9** ($C_{95}H_{89}N_{17}O_{15}$, found/calcd): C, 66.02/66.77; H, 5.20/5.25; N, 13.76/13.93%; for **SOF-10** ($C_{80}H_{76}N_{18}O_{16}$, found/calcd): C, 61.42/62.17; H, 4.88/4.96; N, 15.99/16.31%. IR (KBr, υ_{max}, cm^{-1}) for **SOF-8**: 1943 (w), 1707 (s), 1662 (s), 1608 (m), 1529 (s), 1426 (w), 1390 (s), 1318 (m), 1248 (s), 1145 (w), 1101 (w), 1016 (m), 904 (w), 845 (m), 766 (m), 692 (w), 609 (w), 574 (w), 500 (w); **SOF-9**: 1944 (w) 1712 (s), 1601 (m), 1529 (s), 1447 (w), 1418 (w), 1393 (m), 1269 (s), 1114 (w), 1061 (w), 1022 (w),

DOI: 10.1021/acs.cgd.8b00153
Cryst. Growth Des. 2018, 18, 2555−2562

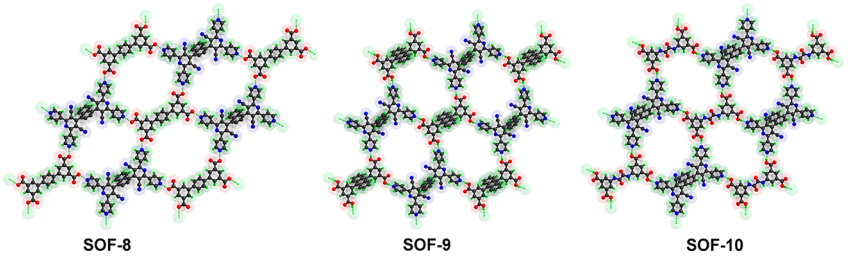

Figure 1. Views of the **hcb** layers in **SOF 8–10**.

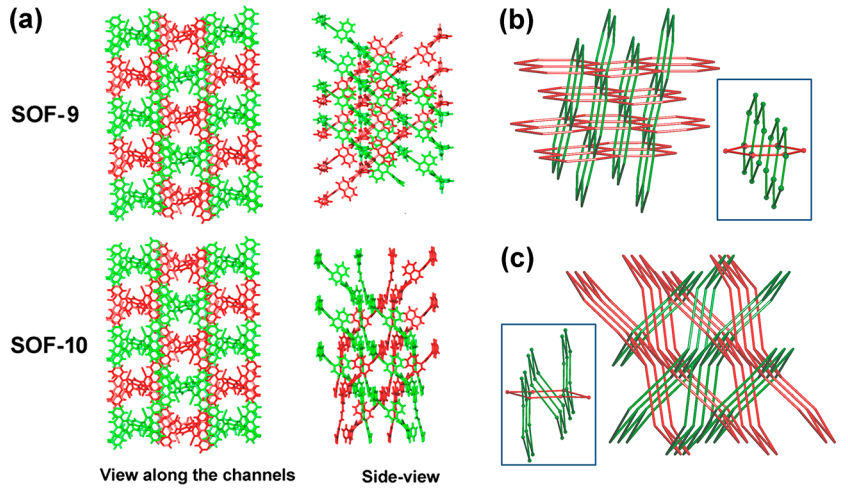

Figure 2. (a) Packing patterns of the polycatenated **SOF-9** and **SOF-10**; parallel layers are presented in the same color. (b) Topological representation of the polycatenated **hcb** layers in **SOF-9** and (c) **SOF-10** (insets: views of the Hopf links).

840 (m), 792 (m), 762 (s), 690 (m), 656 (m), 608 (w), 574 (w), 507 (w); **SOF-10**: 1923 (w), 1709 (s), 1670 (s), 1597 (w), 1530 (s), 1440 (m), 1384 (s), 1322 (w), 1255 (s), 1097 (m), 1064 (m), 1019 (m), 939 (w), 839 (m), 778 (m), 688 (m), 592 (m), 502 (m).

Sample Activation. DMF molecules within the pores of **SOF 8–10** were exchanged with acetone, and the acetone-exchanged samples were degassed under dynamic vacuum at 100 °C for 24 h to afford the activated desolvated samples **SOF 8a–10a**. Thermal stability of as-prepared **SOF 8–10** was evaluated by thermogravimetric analysis (TGA, Figure S1). The phase purity of as-prepared **SOF 8–10** and activated **SOF 8a–10a** was confirmed by powder X-ray diffraction (PXRD, Figures S2–S4). **SOF-9a** and **SOF-10a** possess highly robust frameworks, while structural collapse occurs during activation of **SOF-8** to afford amorphous **SOF-8a**.

Crystallography. Single crystal X-ray data were collected on an Rigaku Oxford Diffraction SuperNovaII Atlas X-ray diffractometer at the University of Nottingham. Details of the data collection are included in the CIF files. Structures of **SOF 8–10** were solved by direct methods and developed by difference Fourier techniques, using the SHELXL software package (Table S1).[38] Hydrogen atoms of the ligands were placed geometrically and refined using a riding model. The unit cell volume of **SOF 8–10** included a large region of disordered solvent which could not be modeled as discrete atomic sites. We therefore employed PLATON/SQUEEZE[37] to calculate the contribution of the solvent region to the diffraction and thereby produced a set of solvent-free diffraction intensities. The solvent molecules of **SOF 8–10** are included in the unit cell contents and in all parameters derived from these. Despite multiple attempts, the limited crystal size and stability of **SOF-8** restricted the quality of the resulting data set, but this did not preclude the identification of the framework structure. Topological analysis and polycatenation identification of **SOF-9** and **SOF-10** were performed using ToposPro software.[39]

RESULTS AND DISCUSSION

Structural Description. In a typical procedure, reaction of **1** and **3** in a 1:1 molar ratio in dimethylformamide (DMF) at 90 °C resulted in the formation of light-yellow prismatic crystals of **SOF-8** after 72 h. Single crystal X-ray diffraction reveals that **SOF-8** crystallizes in the monoclinic space group $P2_1/m$ (Table S1), and features a 2D hydrogen-bonded network structure in which **1** has undergone a structural transformation into **2** through oxidative dehydrogenation (Scheme 1). The *exo*-pyridyl and carboxyl groups on **2** and **3** contribute to the complementary O–H···N hydrogen bonds that direct the self-assembly process. Each molecule of **2** interacts with four neighboring molecules of **3** through strong primary hydrogen bonds ($O_{carboxyl}H\cdots N_{pyridyl}$, 2.562/2.568 Å; Table S2) to form a 2D honeycomb layer (6^3-**hcb**) supramolecular organic framework with windows of *ca.* 10.1 Å × 15.9 Å (Figure 1, left). The 2D 6^3-**hcb** layers stack in a parallel fashion and give rise to an overall 3D supramolecular structure with one-dimensional cyano-decorated channels (Figure S5, Supporting Information). It should be noted that the naphthalene moieties on **2** are disordered in symmetric positions, resulting in them pointing up and down into the windows of the 2D layers. In this way, neighboring 2D layers in **SOF-8** interact with each other via $\pi\cdots\pi$ interactions.

Single crystal X-ray analysis confirms that **SOF-9** crystallizes as a 1:1 mixture of **2** and **4** in the orthorhombic space group *Pba*2 (Table S1). The 2D honeycomb layer subunit in **SOF-9** is built by primary O–H···N hydrogen bonds between *exo*-pyridyl and carboxyl groups on **2** and **4** (Figure 1, middle), hydrogen bonds characterized by O···N distances in the range 2.548–2.633 Å, and approximately linear O–H···N angles (Table S2).

DOI: 10.1021/acs.cgd.8b00153
Cryst. Growth Des. 2018, 18, 2555–2562

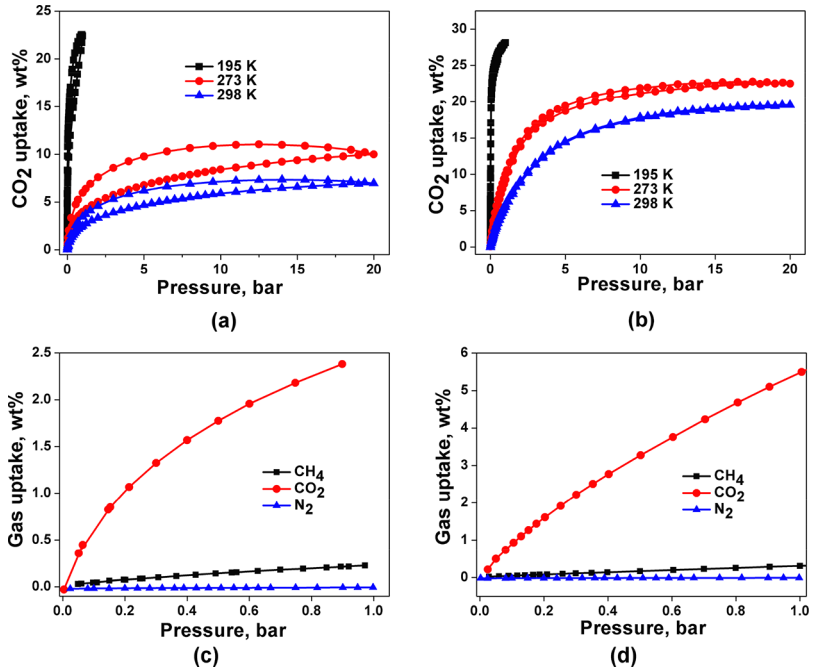

Figure 3. Adsorption/desorption isotherms for CO_2 in **SOF-9a** (a) and **SOF-10a** (b) at 195 K (black), 273 K (red), and 298 K (blue) in the pressure range 0−20 bar; selectivity of CO_2 adsorption over CH_4 and N_2 at 298 K for **SOF-9a** (c) and **SOF-10a** (d).

In comparison with **SOF-8**, windows of the 2D layers in **SOF-9** are more regular, with dimensions of *ca.* 12.0 Å × 12.3 Å. Packing of the 2D layers generates two sets of **hcb** layers,[40−43] resulting in a 3D inclined polycatenated framework (Figure 2a,b). The dihedral angle between these two sets of layers is 79.6°. Each window of a layer is polycatenated with four other windows from two different layers via Hopf links.[39,44] Alternatively, it can be described that each window encircles two edges passing through it (Figure 2b, inset).

X-ray crystallography confirms that **SOF-10** crystallizes in the orthorhombic space group $Pbc2_1$ (Table S1) and comprises **2** and **5** in a 1:1 ratio (Scheme 1). A 2D honeycomb layer with windows of *ca.* 12.1 Å × 14.2 Å is constructed by complementary O−H···N hydrogen bonds between *exo*-pyridyl and carboxyl groups on **2** and **5**, respectively ($O_{carboxyl}H\cdots N_{pyridyl}$, 2.547−2.627 Å; Figure 1, right; Table S1, Supporting Information). Packing of the 2D layers results in a 3D inclined polycatenated framework similar to that of **SOF-9**, consisting of two sets of equivalent **hcb** layers (Figure 2a,c). The dihedral angle between these two sets of layers is 59.5°. Each window of a layer is polycatenated with six windows from three different layers via Hopf links. Alternatively, each window can be described as encircling the three edges passing through it (Figure 2c, inset). It should be noted that the O−H···N hydrogen bonds in **SOF 8−10** are considerably shorter than the ordinary H-bond (2.70−3.00 Å), and they are thus considered as double charge-assisted H-bonds, comprised of strong $^{1/2-}D\cdots H^{+}\cdots A^{1/2-}$ interactions (D = H-bond donor; A = H-bond acceptor).[45,46]

Adsorption and Selectivity. The total solvent-accessible volume of **SOF 8−10** after removal of guest DMF molecules was estimated to be *ca.* 39.2%, 34.2%, and 29.9%, respectively, as calculated using the PLATON/VOID routine.[37] It is not surprising that nonentangled **SOF-8** has the largest potential molecular voids, and the decrease of molecular voids for **SOF-9** and **SOF-10** is attributable to framework interpenetration. However, structural collapse occurs upon removal of guest DMF molecules from **SOF-8** (Figures S1 and S2, Supporting Information). In contrast, the polycatenated **SOF-9** and **SOF-10** display excellent thermal stability, as evaluated by thermogravimetric analysis (TGA) and powder X-ray diffractions (PXRD) (Figures S1, S3, and S4, Supporting Information), and they retain their structural integrity and crystallinity upon solvent exchange as well as upon the removal of guest molecules.

Encouraged by the above observations, we have confirmed the permanent porosity of the activated samples **SOF-9a** and **SOF-10a** by gas adsorption studies. The results clearly show that **SOF-9a** and **SOF-10a** exhibit selective adsorption for CO_2 over N_2 and CH_4. The CO_2 adsorption isotherms of **SOF-9a** and **SOF-10a** recorded at 195, 273, and 298 K (Figure 3a,b) reveal type-I sorption behavior and surface areas of 181.5 and 221.1 $m^2\ g^{-1}$, respectively, comparable to the results for some hydrogen-bonded organic framework and organic molecular solids with intrinsic porosity (Table S3).[6,11,26,47] At 1 bar, **SOF-9a** shows reversible CO_2 adsorption capacities of 4.09 wt % (0.93 mmol g^{-1}) and 2.43 wt % (0.55 mmol g^{-1}) at 273 and 298 K, respectively (Figure 3a). High pressure (20 bar) CO_2 adsorption studies of **SOF-9a** give the total capacities of 10.0 wt % (2.27 mmol g^{-1}) and 6.96 wt % (1.58 mmol g^{-1}) at 273 and 298 K, respectively (Figure 3a), comparable to the CO_2 adsorption capacity of **TBC[4]DHQ** at a higher pressure (35 bar) despite **SOF-9a** having a considerably smaller surface area.[6,48] At 1 bar, **SOF-10a** shows reversible CO_2 adsorption capacities of 9.28 wt % (2.11 mmol g^{-1}) and 5.67 wt % (1.29 mmol g^{-1}) at 273 and 298 K, respectively (Figure 3b). High pressure (20 bar) CO_2 adsorption studies of **SOF-10a** give the total capacities of 22.49 wt % (5.11 mmol g^{-1}) and 19.55 wt % (4.44 mmol g^{-1}) at 273 and 298 K (Figure 3b), respectively. The CO_2 adsorption capacity of **SOF-10a** is superior to that of porous organic molecular solids with comparable surface area, as well as to that of the single-component **SOF-1a** that shows a much higher surface area (474 $m^2\ g^{-1}$). It is notable that the CO_2 adsorption capacity of **SOF-10a** is comparable to that of

DOI: 10.1021/acs.cgd.8b00153
Cryst. Growth Des. 2018, 18, 2555−2562

the only other binary SOF material documented so far, **SOF-7a** (Table S3), which has a surface area more than 4 times that of **SOF-10a**. The enhanced CO_2 adsorption capacity of **SOF-10a** is attributable to the presence of oxamide groups, which function as favorable binding sites for guest CO_2 molecules.[25,49−52] The heat of adsorption for CO_2 (Q_{st}) was calculated via the Clausius−Clapeyron equation using CO_2 isotherms at 273 and 298 K (Figures S6 and S7, Supporting Information) and was found to be 31.9 kJ mol^{-1} for **SOF-9a** and 27.1 kJ mol^{-1} for **SOF-10a**) (Figure S8, Supporting Information), which are slightly higher values than previously reported for single-component SOF materials but comparable to many MOF materials (25−35 kJ mol^{-1}).[13,15,24,26,27,53,54]

In order to evaluate the CO_2 adsorption selectivity, uptake of CH_4 by **SOF-9a** and **SOF-10a** was tested at pressures of up to 20 bar (Figure S9) at 273 and 298 K. **SOF-9a** shows CH_4 uptake of 1.42 wt % (0.89 mmol g^{-1}, 273 K) and 0.73 wt % (0.46 mmol g^{-1}, 298 K) at 20 bar, whereas **SOF-10a** displays significantly higher CH_4 uptake of 3.40 wt % (2.13 mmol g^{-1}, 273 K) and 2.74 wt % (1.71 mmol g^{-1}, 298 K) at the same pressure (Figure S7). Notably, the CH_4 adsorption capacity of **SOF-10a** at 298 K is comparable to those of **SOF-1a** (1.43 mmol·g^{-1}) and **SOF-7a** (1.71 mmol·g^{-1}). In comparison with the selectivity of CO_2 over CH_4 calculated for **SOF-1a** and **SOF-7a** from the Henry's Law, **SOF-9a** and **SOF-10a** exhibit higher CO_2/CH_4 selectivity than **SOF-1a** but lower selectivity than **SOF-7a** (Table S4). The order of CO_2 adsorption is **SOF-1a** < **SOF-9a** < **SOF-10a** < **SOF-7a**, whereas the CO_2 selectivity follows an order of **SOF-1a** < **SOF-10a** < **SOF-9a** < **SOF-7a**.

Quantum Chemical Modeling. In order to gain more insight into these new 2D SOF materials, and to understand why **SOF-9** and **SOF-10** are, like **SOF-7**,[25] stable upon guest removal while **SOF-8** is not, we analyzed these structures by means of quantum chemistry calculations, at the density functional theory (DFT) level. Starting from the guest-free crystallographic structures, geometry optimization was performed first to check that these materials, together with **SOF-7**, are well described at this level of theory, and then focused on their energetic and mechanical stabilities, as well as on vibrational properties. The relaxed structures are in excellent agreement with those obtained by single crystal X-ray crystallography, with deviations below 2% (even below 1% for **SOF-8** and **SOF-10**) in either volume or individual cell parameters, as shown in Table S5. Intermolecular binding via $O_{carboxyl}H\cdots N_{pyridyl}$ bonds is well reproduced, with O···H···N distances between 2.52 and 2.57 Å, although slightly shorter than observed in the experimental structures for **SOF-9** and **SOF-10**.

For each of the relaxed structures, the binding energy (or formation enthalpy) has been estimated by subtracting from the total energy (appropriately weighted) that of its constituting tectons. These binding energies have been found to be all fairly large, between −429 and −438 kJ mol^{-1} (per carboxylate-based constituent). It should be noted that these refer to the formation of SOF materials in the absence of solvents; we expect the formation enthalpies of these materials in DMF to be significantly smaller, since a rather large binding energy of DMF to carboxylate-based constituents (calculated binding energy as −65 to −80 kJ mol^{-1}, depending on the constituent) is essentially lost when this constituent binds to an *exo*-pyridyl group.

The mechanical properties of these SOF materials have also been investigated by means of computing their second-order elastic stiffness tensors (also known as elastic constants). This has proven to be a reliable indicator of mechanical stability and potential for crystal-to-crystal phase transitions in metal−organic frameworks and other framework materials.[55−57] The resulting bulk, Young's, and shear moduli are listed in Table S6. All materials have reasonably large bulk moduli, between 9.0 and 9.5 GPa. Their response to isostatic pressure is however unusual, with (small) negative linear compressibility in specific directions. Whereas spatially averaged Young's moduli E, ranging from 5.8 GPa in **SOF-7** to 9.0 GPa in **SOF-10**, do not differ much from one material to another, their response to directional strains is instructive. Some materials are particularly soft with respect to specific deformation modes, especially the shear moduli which can be very low, G_{min} = 0.21 GPa for **SOF-7** and 0.41 GPa for **SOF-8**. Both materials are also sensitive to specific compression modes with E_{min} of the order of 1 GPa or below. For instance, the soft shearing mode of **SOF-8** corresponds to sliding of a 2D honeycomb layer with respect to neighboring layers. Its counterpart in **SOF-7** is similar, implicating relative motions of neighboring constituents, although the situation is slightly more complex since neighboring coordination layers are intertwined.[25] The higher stability of **SOF-8** over **SOF-7** to shearing deformations, from these results, seems inconsistent with higher stability of **SOF-7** to desolvation, which might induce some local deformations. An important difference, however, is that **SOF-7** consists of intertwined networks (as do **SOF-9** and **SOF-10**), which may result in a higher stability to large deformations (beyond the elastic regime), compared to the essentially layered **SOF-8**. A similar behavior has been observed, for example, in the family of **MUF-8** and **MUF-9** metal−organic frameworks with controlled partial interpenetration.[58]

Vibration modes of **SOF-7** and **SOF-8** have been further analyzed. For the latter, a large number of low-frequency modes are found: eight modes with frequencies ω < 30 cm^{-1} (not including three purely translational modes), and about 50 modes spread quite regularly over the range of 30−100 cm^{-1}. An analysis of the former eight gives the following trends:

(a) In two of these modes, constituents vibrate as (almost) rigid units, and their motion involves significant deformations in the O−H···N units (shortening/elongation of O−H or N···H bonds).

(b) In the two other modes, constituents from the same coordination layer vibrate in phase, but such that neighboring layers slide with respect to each other. This induces local deformations, e.g., bending of C−C−C angles at tertiary carbons, and relative motions of neighboring aromatic cycles coupled by $\pi\cdots\pi$ interactions.

(c) The remaining four modes have more complex structures, involving significant bending of C−C−C angles at tertiary carbons and/or of dihedrals centered on single C−C bonds between aromatic rings.

Similarly, **SOF-7** has a large number of low-frequency vibration modes, but fewer (in comparison to **SOF-8**) in the ω < 20 cm^{-1} range. Moreover, modes of the type (c), connected to the polycatenated nature of the framework, are again absent for **SOF-7**. This qualitative difference, as well as the larger population of vibration modes in **SOF-8** at ambient temperature, may explain its instability upon desolvation.

DOI: 10.1021/acs.cgd.8b00153
Cryst. Growth Des. 2018, 18, 2555−2562

Finally, vibrational mode calculations at finite (positive and negative) pressures have been performed in order to determine the thermal expansion coefficients $\alpha_V = V^{-1}$ (dV/dT). We obtained the values α_V = 15.7 MK^{-1} for **SOF-7**, and a remarkably low α_V = 2.2 MK^{-1} for **SOF-8**. The latter value is due to the presence, among low-energy vibration modes, of several modes that tend to soften (decrease in frequency) under compression; i.e., these modes alone would result in negative thermal expansion (NTE). This makes it likely that NTE will be encountered in further SOF materials, which opens further perspectives for applications of these materials.

CONCLUSION

In summary, we have demonstrated a rational design strategy to prepare 2D binary supramolecular organic framework (SOF) materials assembled via complementary hydrogen bonding interactions. The SOF assembly is tunable through rational design of organic constituents with hydrogen bond donating and accepting groups. The porous supramolecular organic frameworks **SOF 8−10** display similar 2D hydrogen-bonded 6^3-**hcb** layers with various packing modes: **SOF-8** features parallel packing of 2D layers, whereas **SOF-9** and **SOF-10** possess 2D → 3D inclined polycatenation of 6^3-**hcb** layers. The higher chemical and thermal stability for **SOF-9** and **SOF-10**, which are stable up to 300 °C, have been achieved through structural polycatenation. Further enhancement of adsorption capacity in activated samples of **SOF-10a** depends greatly on the introduction of favorable binding sites (the oxamide group in this case) for guest CO_2 molecules. Therefore, appropriate functionalization of the organic constituents in SOF materials favors not only the stability of the materials but also their gas adsorption capacity and selectivity. Quantum chemistry calculations suggest a connection between this stability and the existence of soft deformation modes (especially shearing modes) and low-energy vibration modes. The latter may in particular account for the instability of **SOF-8** upon guest removal, and also for unusual thermal expansion properties. These results further confirm that our binary design strategy is effective for the synthesis of highly stable and robust functional porous supramolecular organic framework materials with potentials for storage and separation. Moreover, enhanced CO_2 adsorption and selectivity has been achieved by structural regulation via controlled assembly of 2D SOF materials into polycatenated structures.

ASSOCIATED CONTENT

Supporting Information

The Supporting Information is available free of charge on the ACS Publications website at DOI: 10.1021/acs.cgd.8b00153.

Gas adsorption isotherms, gas uptake data and analysis, and quantum chemistry calculations, tables, and figures (PDF)

Accession Codes

CCDC 1818274−1818276 contain the supplementary crystallographic data for this paper. These data can be obtained free of charge via www.ccdc.cam.ac.uk/data_request/cif, or by emailing data_request@ccdc.cam.ac.uk, or by contacting The Cambridge Crystallographic Data Centre, 12 Union Road, Cambridge CB2 1EZ, UK; fax: +44 1223 336033.

AUTHOR INFORMATION

Corresponding Authors

*E-mail: m.schroder@manchester.ac.uk (M.S.).
*E-mail: rcao@fjirsm.ac.cn (R.C.).

ORCID

Jian Lü: 0000-0002-0015-8380
William Lewis: 0000-0001-7103-6981
François-Xavier Coudert: 0000-0001-5318-3910
Rong Cao: 0000-0003-2384-791X
Martin Schröder: 0000-0001-6992-0700

Notes

The authors declare no competing financial interest.
Correspondence and requests for materials should be addressed to F-X.C., R.C., and M.S.

ACKNOWLEDGMENTS

We thank the EPSRC (EP/I011870), ERC (Advanced Grant AdG 226593), the 973 program (Grant 2014CB845605), the NSFC (Grants 91622114, 21520102001, and 21521061), the Strategic Priority Research Program (Grants XDB20000000 and XDA09030102) of the Chinese Academy of Sciences for funding. J.L. acknowledges financial support from the International Science and Technology Cooperation and Exchange Project of Fujian Agriculture and Forestry University (Grant No. KXGH17010). F.T. and F.-X.C. acknowledge access to high-performance computing platforms provided by a GENCI grant (A0030807069).

REFERENCES

(1) Brändle, M.; Sauer, J. Acidity differences between inorganic solids induced by their framework structure. A combined quantum mechanics/molecular mechanics ab initio study on zeolites. *J. Am. Chem. Soc.* **1998**, *120*, 1556−1570.

(2) Yang, Z.; Xia, Y.; Mokaya, R. Enhanced hydrogen storage capacity of high surface area aeolite-like carbon materials. *J. Am. Chem. Soc.* **2007**, *129*, 1673−1679.

(3) Hao, G.-P.; Li, W.-C.; Qian, D.; Lu, A.-H. Rapid synthesis of nitrogen-doped porous carbon monolith for CO_2 capture. *Adv. Mater.* **2010**, *22*, 853−857.

(4) Hao, G.-P.; Li, W.-C.; Qian, D.; Wang, G.-H.; Zhang, W.-P.; Zhang, T.; Wang, A.-Q.; Schüth, F.; Bongard, H.-J.; Lu, A.-H. Structurally designed synthesis of mechanically stable poly(benzoxazine-co-resol)-based porous carbon monoliths and their application as high-performance CO_2 capture sorbents. *J. Am. Chem. Soc.* **2011**, *133*, 11378−11388.

(5) Hudson, M. R.; Queen, W. L.; Mason, J. A.; Fickel, D. W.; Lobo, R. F.; Brown, C. M. Unconventional, highly selective CO_2 adsorption in zeolite SSZ-13. *J. Am. Chem. Soc.* **2012**, *134*, 1970−1973.

(6) Msayib, K. J.; Book, D.; Budd, P. M.; Harris, K. D. M.; Helliwell, M.; Tedds, S.; Warren, J. E.; Xu, M. C.; McKeown, N. B.; Chaukura, N.; Walton, A. Nitrogen and hydrogen adsorption by an organic microporous crystal. *Angew. Chem., Int. Ed.* **2009**, *48*, 3273−3277.

(7) Trewin, A.; Cooper, A. I. Porous organic polymers: distinction from disorder? *Angew. Chem., Int. Ed.* **2010**, *49*, 1533−1535.

(8) Ben, T.; Pei, C.; Zhang, D.; Xu, J.; Deng, F.; Jing, X.; Qiu, S. Gas storage in porous aromatic frameworks (PAFs). *Energy Environ. Sci.* **2011**, *4*, 3991−3999.

(9) Bezzu, C. G.; Carta, M.; Tonkins, A.; Jansen, J. C.; Bernardo, P.; Bazzarelli, F.; McKeown, N. B. A spirobifluorene-based polymer of intrinsic microporosity with improved performance for gas separation. *Adv. Mater.* **2012**, *24*, 5930−5933.

(10) Ding, S.-Y.; Wang, W. Covalent organic frameworks (COFs): from design to applications. *Chem. Soc. Rev.* **2013**, *42*, 548−568.

DOI: 10.1021/acs.cgd.8b00153
Cryst. Growth Des. 2018, 18, 2555−2562

(11) Sozzani, P.; Bracco, S.; Comotti, A.; Ferretti, L.; Simonutti, R. Methane and carbon dioxide storage in a porous van der Waals crystal. *Angew. Chem., Int. Ed.* **2005**, *44*, 1816−1820.
(12) He, Y.; Xiang, S.; Chen, B. A microporous hydrogen-bonded organic framework for highly selective C_2H_2/C_2H_4 separation at ambient temperature. *J. Am. Chem. Soc.* **2011**, *133*, 14570−14573.
(13) Mastalerz, M.; Oppel, I. M. Rational construction of an extrinsic porous molecular crystal with an extraordinary high specific surface area. *Angew. Chem., Int. Ed.* **2012**, *51*, 5252−5255.
(14) Luo, X.-Z.; Jia, X.-J.; Deng, J.-H.; Zhong, D.-C.; Liu, H.-J.; Wang, K.-J.; Zhong, D.-C. A microporous hydrogen-bonded organic framework: exceptional stability and highly selective adsorption of gas and liquid. *J. Am. Chem. Soc.* **2013**, *135*, 11684−11687.
(15) Li, P.; He, Y.; Guang, J.; Weng, L.; Zhao, J. C.-G.; Xiang, S.; Chen, B. A homochiral microporous hydrogen-bonded organic framework for highly enantioselective separation of secondary alcohols. *J. Am. Chem. Soc.* **2014**, *136*, 547−549.
(16) Yamamoto, A.; Hamada, T.; Hisaki, I.; Miyata, M.; Tohnai, N. Dynamically deformable cube-like hydrogen-bonding networks in water-responsive diamondoid oorous organic salts. *Angew. Chem., Int. Ed.* **2013**, *52*, 1709−1712.
(17) Li, P.; He, Y.; Zhao, Y.; Weng, L.; Wang, H.; Krishna, R.; Wu, H.; Zhou, W.; O'Keeffe, M.; Han, Y.; Chen, B. A rod-packing microporous hydrogen-bonded organic framework for highly selective separation of C_2H_2/CO_2 at room temperature. *Angew. Chem., Int. Ed.* **2015**, *54*, 574−577.
(18) Wang, H.; Li, B.; Wu, H.; Hu, T.-L.; Yao, Z.; Zhou, W.; Xiang, S.; Chen, B. A flexible microporous hydrogen-bonded organic framework for gas sorption and separation. *J. Am. Chem. Soc.* **2015**, *137*, 9963−9970.
(19) Zhang, J. P.; Chen, X. M. Optimized acetylene/carbon dioxide sorption in a dynamic porous crystal. *J. Am. Chem. Soc.* **2009**, *131*, 5516−5521.
(20) Sumida, K.; Rogow, D. L.; Mason, J. A.; McDonald, T. M.; Bloch, E. D.; Herm, Z. R.; Bae, T.-H.; Long, J. R. Carbon dioxide capture in metal-organic frameworks. *Chem. Rev.* **2012**, *112*, 724−781.
(21) Yang, S.; Lin, X.; Lewis, W.; Suyetin, M.; Bichoutskaia, E.; Parker, J.; Tang, C. C.; Allan, D. R.; Rizkallah, P. J.; Hubberstey, P.; Champness, N. R.; Thomas, K. M.; Blake, A. J.; Schröder, M. A partially interpenetrated metal-organic framework for selective hysteretic sorption of carbon dioxide. *Nat. Mater.* **2012**, *11*, 710−716.
(22) Yang, S.; Sun, J.; Ramirez-Cuesta, A. J.; Callear, S. K.; David, W. I. F.; Anderson, D.; Newby, R.; Blake, A. J.; Parker, J. E.; Tang, C. C.; Schröder, M. Selectivity and direct visualization of carbon dioxide and sulfur dioxide in a decorated porous host. *Nat. Chem.* **2012**, *4*, 887−849.
(23) Zhu, X.-D.; Zhang, K.; Wang, Y.; Long, W.-W.; Sa, R.-J.; Liu, T.-F.; Lü, J. Fluorescent metal organic framework (MOF) as a highly sensitive and quickly responsive chemical sensor for the detection of antibiotics in simulated wastewater. *Inorg. Chem.* **2018**, *57*, 1060−1065.
(24) Yang, W.; Greenaway, A.; Lin, X.; Matsuda, R.; Blake, A. J.; Wilson, C.; Lewis, W.; Hubberstey, P.; Kitagawa, S.; Champness, N. R.; Schröder, M. Exceptional thermal stability in a supramolecular organic framework: porosity and gas storage. *J. Am. Chem. Soc.* **2010**, *132*, 14457.
(25) Lü, J.; Perez-Krap, C.; Suyetin, M.; Alsmail, N. H.; Yan, Y.; Yang, S.; Lewis, W.; Bichoutskaia, E.; Tang, C. C.; Blake, A. J.; Cao, R.; Schröder, M. A robust binary supramolecular organic framework (SOF) with high CO_2 adsorption and selectivity. *J. Am. Chem. Soc.* **2014**, *136*, 12828−12831.
(26) Kim, H.; Kim, Y.; Yoon, M.; Lim, S.; Park, S. M.; Seo, G.; Kim, K. Highly selective carbon dioxide sorption in an organic molecular porous material. *J. Am. Chem. Soc.* **2010**, *132*, 12200−12202.
(27) Tian, J.; Ma, S.; Thallapally, P. K.; Fowler, D.; McGrail, B. P.; Atwood, J. L. Cucurbit[7]uril: an amorphous molecular material for highly selective carbon dioxide uptake. *Chem. Commun.* **2011**, *47*, 7626−7628.
(28) Zhang, K.-D.; Tian, J.; Hanifi, D.; Zhang, Y.; Sue, A. C.-H.; Zhou, T.-Y.; Zhang, L.; Zhao, X.; Liu, U.; Li, Z.-T. Toward a single-layer two-dimensional honeycomb supramolecular organic framework in water. *J. Am. Chem. Soc.* **2013**, *135*, 17913−17918.
(29) Hisaki, I.; Nakagawa, S.; Ikenaka, N.; Imamura, Y.; Katouda, M.; Tashiro, M.; Tsuchida, H.; Ogoshi, T.; Sato, H.; Tohnai, N.; Miyata, M. A series of layered assemblies of hydrogen-bonded, hexagonal networks of C_3-symmetric π-conjugated molecules: A potential motif of porous organic materials. *J. Am. Chem. Soc.* **2016**, *138*, 6617−6628.
(30) Martí-Rujas, J.; Colombo, L.; Lü, J.; Dey, A.; Terraneo, G.; Metrangolo, P.; Pilati, T.; Resnati, G. Hydrogen and halogen bonding drive the orthogonal self-assembly of an organic framework possessing 2D channels. *Chem. Commun.* **2012**, *48*, 8207−8209.
(31) Bhogala, B. R.; Basavoju, S.; Nangia, A. Three-component carboxylic acid-bipyridine lattice inclusion host. Supramolecular synthesis of ternary cocrystals. *Cryst. Growth Des.* **2005**, *5*, 1683−1686.
(32) Huang, Y.-G.; Shiota, Y.; Wu, M.-Y.; Su, S.-Q.; Yao, Z.-S.; Kang, S.; Kanegawa, S.; Li, G.-L.; Wu, S.-Q.; Kamachi, T.; Yoshizawa, K.; Ariga, K.; Hong, M.-C.; Sato, O. Superior thermoelasticity and shape-memory nanopores in a porous supramolecular organic framework. *Nat. Commun.* **2016**, *7*, 11564.
(33) Hill, R. J.; Long, D.-L.; Champness, N. R.; Hubberstey, P.; Schröder, M. New approaches to the analysis of high connectivity materials: Design frameworks based upon 4^4- and 6^3-subnet tectons. *Acc. Chem. Res.* **2005**, *38*, 335−348.
(34) Lü, J.; Han, L.-W.; Alsmail, N. H.; Blake, A. J.; Lewis, W.; Cao, R.; Schröder, M. Control of assembly of dihydropyridyl and pyridyl molecules via directed hydrogen bonding. *Cryst. Growth Des.* **2015**, *15*, 4219−4224.
(35) Schaate, A.; Roy, P.; Godt, A.; Lippke, J.; Waltz, F.; Wiebcke, M.; Behrens, P. Modulated synthesis of Zr-based metal-organic frameworks: from nano to single crystals. *Chem. - Eur. J.* **2011**, *17*, 6643−6651.
(36) Hauptvogel, I. M.; Biedermann, R.; Klein, N.; Senkovska, I.; Cadiau, A.; Wallacher, D.; Feyerherm, R.; Kaskel, S. Flexible and hydrophobic Zn-based metal-organic framework. *Inorg. Chem.* **2011**, *50*, 8367−8374.
(37) Spek, A. L. Structure validation in chemical crystallography. *Acta Crystallogr., Sect. D: Biol. Crystallogr.* **2009**, *65*, 148−155.
(38) Sheldrick, G. M. A short history of SHELX. *Acta Crystallogr., Sect. A: Found. Crystallogr.* **2008**, *64*, 112−122.
(39) Blatov, V. A.; Shevchenko, A. P.; Proserpio, D. M. Applied topological analysis of crystal structures with the program package *ToposPro*. *Cryst. Growth Des.* **2014**, *14*, 3576−3586.
(40) Carlucci, L.; Ciani, G.; Proserpio, D. M. Polycatenation, polythreading and polyknotting in coordination network chemistry. *Coord. Chem. Rev.* **2003**, *246*, 247−289.
(41) Proserpio, D. M. Topological crystal chemistry: polycatenation weaves a 3D web. *Nat. Chem.* **2010**, *2*, 435−436.
(42) Zentner, C. A.; Lai, H. W. H.; Greenfield, J. T.; Wiscons, R. A.; Zeller, M.; Campana, C. F.; Talu, O.; FitzGerald, S. A.; Rowsell, J. L. C. High surface area and Z′ in a thermally stable 8-fold polycatenated hydrogen-bonded framework. *Chem. Commun.* **2015**, *51*, 11642−10645.
(43) Lai, H. W. H.; Wiscons, R. A.; Zentner, C. A.; Zeller, M.; Rowsell, J. L. C. Supramolecular assembly of tris(4-carboxyphenyl)-arenes: Relationship between molecular structure and solid-state catenation motifs. *Cryst. Growth Des.* **2016**, *16*, 821−833.
(44) Hisaki, I.; Ikenaka, N.; Gomez, E.; Cohen, B.; Tohnai, N.; Douhal, A. Hexaazatriphenylene-based hydrogen-bonded organic framework with permanent porosity and single-crystallinity. *Chem. - Eur. J.* **2017**, *23*, 11611−11619.
(45) Gilli, P.; Pretto, L.; Bertolasi, V.; Gilli, G. Predicting hydrogen-bond strengths from acid-base molecular properties. The pKa slide rule: toward the solution of a long-lasting problem. *Acc. Chem. Res.* **2009**, *42*, 33−44.
(46) Lü, J.; Han, L.-W.; Lin, J.-X.; Liu, T.-F.; Cao, R. Rare Case of a Triple-stranded molecular braid in an organic cocrystal. *Cryst. Growth Des.* **2010**, *10*, 4217−4220.

DOI: 10.1021/acs.cgd.8b00153
Cryst. Growth Des. 2018, 18, 2555−2562

(47) Lü, J.; Cao, R. Porous organic molecular frameworks with extrinsic porosity: A platform for carbon storage and separation. *Angew. Chem., Int. Ed.* **2016**, *55*, 9474−9480.
(48) Thallapally, P. K.; McGrail, B. P.; Atwood, J. L.; Gaeta, C.; Tedesco, C.; Neri, P. Carbon dioxide capture in a self-assembled organic nanochannels. *Chem. Mater.* **2007**, *19*, 3355−3357.
(49) Zheng, B.; Bai, J.; Duan, J.; Wojtas, L.; Zaworotko, M. J. Enhanced CO_2 binding affinity of a high-uptake rht-type metal-organic framework decorated with acylamide groups. *J. Am. Chem. Soc.* **2011**, *133*, 748−751.
(50) Yuan, D. Q.; Zhao, D.; Sun, D. F.; Zhou, H.-C. An isoreticular series of metal-organic frameworks with dendritic hexacarboxylate ligands and exceptionally high gas-uptake capacity. *Angew. Chem., Int. Ed.* **2010**, *49*, 5357−5361.
(51) Park, J.; Li, J.-R.; Chen, Y.-P.; Yu, J.; Yakovenko, A. A.; Wang, Z. U.; Sun, L.-B.; Balbuena, P. B.; Zhou, H.-C. A versatile metal-organic framework for carbon dioxide capture and cooperative catalysis. *Chem. Commun.* **2012**, *48*, 9995−9997.
(52) Alsmail, N. H.; Suyetin, M.; Yan, Y.; Cabot, R.; Krap, C. P.; Lü, J.; Easun, T. L.; Bichoutskaia, E.; Lewis, W.; Blake, A. J.; Schröder, M. Analysis of high and selective uptake of CO_2 in an oxamide containing $\{Cu_2(OOCR)_4\}$-based metal-organic framework. *Chem. - Eur. J.* **2014**, *20*, 7317−7324.
(53) Bourrelly, S.; Llewellyn, P. L.; Serre, C.; Millange, F.; Loiseau, T.; Férey, G. Different adsorption behaviors of methane and carbon dioxide in the isotypic nanoporous metal terephthalates MIL-53 and MIL-47. *J. Am. Chem. Soc.* **2005**, *127*, 13519−13521.
(54) Loiseau, T.; Lecroq, L.; Volkringer, C.; Marrot, J.; Férey, G.; Haouas, M.; Taulelle, F.; Bourrelly, S.; Llewellyn, P. L.; Latroche, M. MIL-96, a porous aluminum trimesate 3D structure constructed from a hexagonal network of 18-membered rings and μ_3-oxo-centered trinuclear units. *J. Am. Chem. Soc.* **2006**, *128*, 10223−10230.
(55) Bouëssel du Bourg, L.; Ortiz, A. U.; Boutin, A.; Coudert, F.-X. Thermal and mechanical stability of zeolitic imidazolate frameworks polymorphs. *APL Mater.* **2014**, *2*, 124110−124119.
(56) Ortiz, A. U.; Boutin, A.; Coudert, F.-X. Prediction of flexibility of metal-organic frameworks CAU-13 and NOTT-300 by first principles molecular simulations. *Chem. Commun.* **2014**, *50*, 5867−5870.
(57) Lin, Y.; Jiang, X.; Kim, S. T.; Alahakoon, S. B.; Hou, X.; Zhang, Z.; Thompson, C. M.; Smaldone, R. A.; Ke, C. An elastic hydrogen-bonded cross-linked organic framework for effective iodine capture in water. *J. Am. Chem. Soc.* **2017**, *139*, 7172−7175.
(58) Ferguson, A.; Liu, L.; Tapperwijn, S. J.; Perl, D.; Coudert, F.-X.; Van Cleuvenbergen, S.; Verbiest, T.; van der Veen, M. A.; Telfer, S. G. Controlled partial interpenetration in metal-organic frameworks. *Nat. Chem.* **2016**, *8*, 250−257.

DOI: 10.1021/acs.cgd.8b00153
Cryst. Growth Des. 2018, 18, 2555−2562